NANO LETTERS

Letter

pubs.acs.org/NanoLett

A Zeptoliter Volume Meter for Analysis of Single Protein Molecules

Tor Sandén,[†] Romain Wyss,[†] Christian Santschi,[‡] Ghérici Hassaïne,[†] Cédric Deluz,[†] Olivier J.F. Martin,[‡] Stefan Wennmalm,[§] and Horst Vogel*[,†]

[†]Laboratory of Physical Chemistry of Polymers and Membranes and [‡]Nanophotonics and Metrology Laboratory, Ecole Polytechnique Fédérale de Lausanne, 1015 Lausanne, Switzerland

[§]Experimental Biomolecular Physics, Department of Applied Physics, Royal Institute of Technology, Stockholm, Sweden

Supporting Information

ABSTRACT: A central goal in bioanalytics is to determine the concentration of and interactions between biomolecules. Nanotechnology allows performing such analyses in a highly parallel, low-cost, and miniaturized fashion. Here we report on label-free volume, concentration, and mobility analysis of single protein molecules and nanoparticles during their diffusion through a subattoliter detection volume, confined by a 100 nm aperture in a thin gold film. A high concentration of small fluorescent molecules renders the aqueous solution in the aperture brightly fluorescent. Nonfluorescent analytes diffusing into the aperture displace the fluorescent molecules in the solution, leading to a decrease of the detected fluorescence signal, while analytes diffusing out of the aperture return the fluorescence level. The resulting fluorescence fluctuations provide direct information on the volume, concentration, and mobility of the nonfluorescent analytes through fluctuation analysis in both time and amplitude.

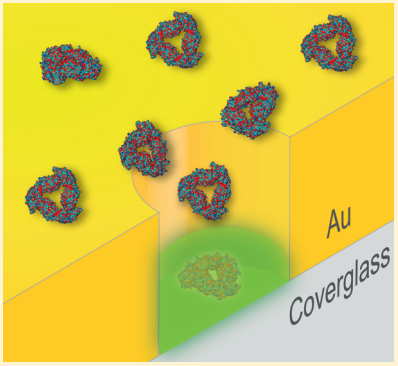

KEYWORDS: *Bioanalysis, label-free, nanostructures, near-field, inverse-fluorescence correlation spectroscopy, intensity distribution analysis, single-molecules*

The field of bioanalytics is experiencing an ever increasing trend toward miniaturization and parallelization driven by novel developments in micro- and nanotechnologies.[1−6] In this context fluorescence-based methods are of central importance thanks to their utmost sensitivity down to single molecules. Although very sensitive and specific, fluorescence techniques normally require labeling which is time-consuming and may influence molecular interactions. For these reasons there is a need for label-free approaches either detecting ensembles of analytes, such as surface plasmon resonance (SPR),[7,8] interferometer-based sensing,[9] dynamic light scattering,[10] and small-angle scattering of X-rays and neutrons,[11] or detecting single molecules/particles either electrically[12−16] or optically.[2,3,17] In the case of the recently developed inverse-fluorescence correlation spectroscopy (iFCS),[17] fluctuations are analyzed in a fluorescent background due to nonfluorescent particles transiently occupying a confocal microscope detection volume. In line with Archimedes' principle, the number of displaced fluorescent molecules by a particle is a direct measure of the particle volume. However, when realized with a femtoliter-sized (10^{-15} l) diffraction-limited confocal excitation/detection volume, iFCS is limited to the analysis of rather large-volume particles (>100 nm diameter).[17]

Confining light in optical microscopy below the diffraction limit has been achieved by, e.g., exploiting photophysical principles in stimulated emission depletion (STED)[18] or by using nanostructured surfaces.[19] Here, subwavelength apertures in plasmonic metal layers were combined with the iFCS displacement principle to enable optical label-free volume, concentration, and motion analysis of nanosized objects, including single protein molecules (Figure 1). This type of apertures has been shown to enhance fluorescence brightness and confine the excitation/detection volume down to zeptoliters (10^{-21} l).[20−23] In our measurements, the number of displaced fluorophores directly scales with the volume of the objects, the frequency of the resulting fluctuations in the detected signal is proportional to the object concentration, and the time that the molecules are displaced is related to the mobility of the objects. Fluctuation analysis (Figure 1b−d) is here not only performed in time as in FCS[24−27] but also in amplitude as in fluorescence intensity distribution analysis (FIDA)[28] or photon counting histograms (PCH).[29]

First, we performed measurements on aqueous solutions containing background fluorophores and fluorescent polystyrene beads of various sizes, in apertures of different diameters (Figure 2). A single aperture was illuminated with two colors using an epi-fluorescence confocal microscope, and fluorescence intensity time traces were recorded for both background and beads. For 24 nm green fluorescent beads in a red fluorescent aqueous solution, transient decreases in intensity in the background channel coincide with positive spikes in the bead channel, evidencing beads traversing the 100 nm aperture (Figure 2a). Fluorescence intensity time traces acquired from a pure fluorophore solution did not display such decreases.

Received: October 16, 2011
Revised: November 30, 2011
Published: December 7, 2011

   dx.doi.org/10.1021/nl2036468 | *Nano Lett.* 2012, 12, 370−375

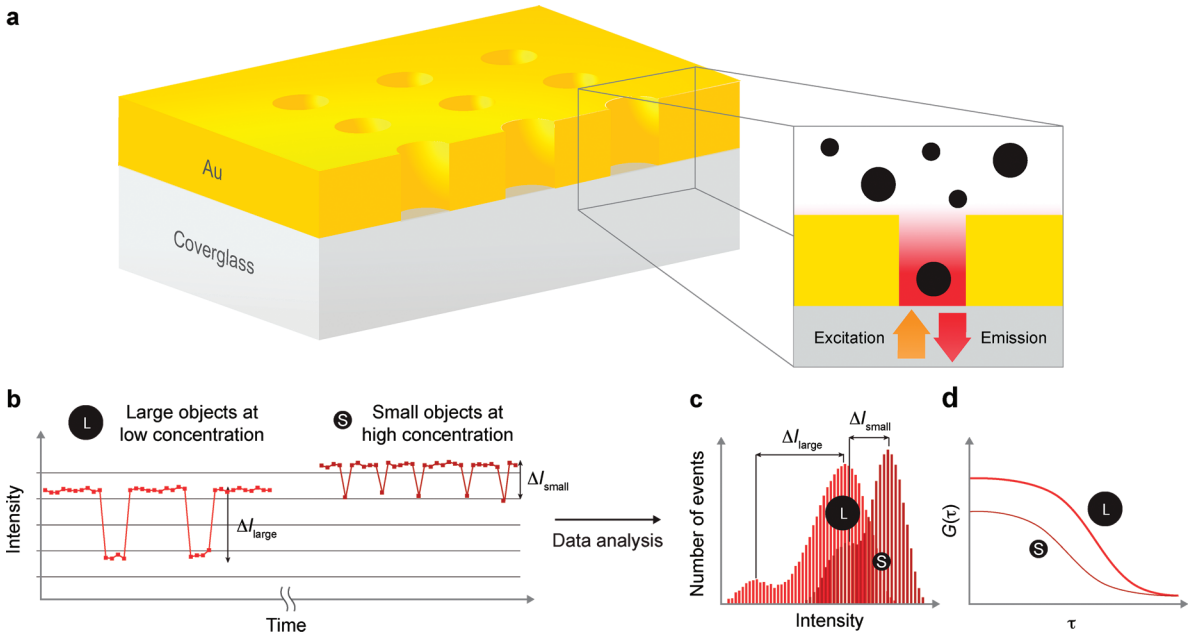

Figure 1. Illustration of our approach. (a) The subwavelength apertures in the gold film on the glass substrate confine the detection volume to zeptoliters (red zone in magnified view). (b) By recording the fluorescence light from background molecules in the detection volume (red and dark red traces), nonfluorescent objects (solid black circles, a)) can be detected when traversing the volume as a decrease in the fluorescence signal (displacing background molecules). The number of displaced background molecules depends on the number N and volume V_{obj} of the nonfluorescent objects. Large objects dwell longer in the aperture and displace a larger number of fluorescent molecules per object than small objects ($\Delta I_{large} > \Delta I_{small}$), and a higher object concentration yields a higher frequency of fluorescence fluctuations. If N on average is <1 and the bin time < dwell time of objects in the detection volume, then $\Delta I \propto V_{obj}$. (c) and (d) Analysis of the fluorescence fluctuations by photon counting histograms and temporal correlations, respectively. The photon counting histograms communicate differences in object volume and concentration through the histogram shape; distance between populations directly relates to object volume and height of population to the concentration. The bin time dependence of the intensity distribution enables access to mobility information.[33] The correlation curve amplitude depends on the volume and concentration of the objects (Supporting Information) and the decay time of the curve on their mobility. The size of objects that can be monitored is limited by the ratio $V_q = V_{obj}/V_{dv}$ and the noise of the background signal, where V_{dv} is the detection volume.[17]

Temporal autocorrelation of the background signal is displayed in Figure 2b (red upper curve). The amplitude of the autocorrelation curve of the background signal is a function of the bead volume, the aperture volume, and the concentration of beads (Figure 2c). The decay time is related to the bead and aperture volumes (Figure S1, Supporting Information). The autocorrelation amplitude of the background signal for three bead sizes linearly increases with bead concentration, as expected from eq S2 (Supporting Information). Fits to the data (Figure 2c) yield an estimate of the effective detection volumes, V_{dv}^{eff}, for the apertures. For 200 nm apertures $V_{dv}^{eff} = 1.8 \pm 0.1 \times 10^{-17}$ liters was obtained using 110 nm beads, 150 nm apertures yielded $V_{dv}^{eff} = 7.5 \pm 0.1 \times 10^{-19}$ liters using 36 nm beads, and 100 nm apertures $V_{dv}^{eff} = 1.2 \pm 0.1 \times 10^{-19}$ liters using 24 nm beads. The estimated V_{dv}^{eff} values are comparable to those obtained by other groups using similar nanostructures.[21,22] However, our estimations have the advantage of not relying on the diffusion time, which can be influenced by temperature, viscosity, and interaction with the nanostructure. The cross-correlation[30] between the background and bead channel (black lower curve in Figure 2b) reveals an anticorrelation,[31,32] and its decay time agrees with that of the autocorrelation. The anticorrelation provides a straightforward way to verify that the decreases in the background signal originate from transiting beads, and its amplitude gives a direct measure of the bead volume to aperture volume ratio[32] (eq S6, Supporting Information).

Intensity distribution analysis was performed in addition to correlation analysis (Supporting Information). A fluorescence intensity histogram of the background signal in Figure 2a reveals two populations originating from the intensity distribution of the background molecules in the absence and presence of beads, respectively (Figure 2d). Fits to the histogram yield the mean values, $I_{background}$ and I_{bead}, of the background and bead intensity distributions, respectively. If the bin time underlying the histogram is in the order of the diffusion time of the beads, the fluctuations in the background signal are smeared out and the I_{bead} shifted toward the background population (inset of Figure 2d). The I_{bead} dependence on the bin time therefore gives an indication of bead mobility.[33] The intensity difference between the two populations, ΔI and knowing V_{dv}^{eff} enables direct estimation of the bead volume:

$$\frac{\Delta I}{I_{background}} = \frac{V_{obj}}{V_{dv}^{eff}} \quad (1)$$

Using $V_{dv}^{eff} = 1.2 \times 10^{-19}$ liters (see above) for 100 nm apertures and ΔI for the shortest bin time yields $V_{bead} = 7.4 \times 10^{-21}$ liters for the 24 nm beads, in good agreement with the calculated 7.2×10^{-21} liters using the known bead diameter. For smaller particles than 24 nm beads, it was found that the volume ratio in eq 1 was too small to be resolved in the histograms due to overlap of populations. Thus, intensity distribution analysis enables direct, model-free determination of the particle volume, without the need for labeled particles as in fluorescence cross-correlation (iFCCS)[32] or multiparameter determination as in iFCS.[17] Additionally, intensity distribution

dx.doi.org/10.1021/nl2036468 | Nano Lett. 2012, 12, 370–375

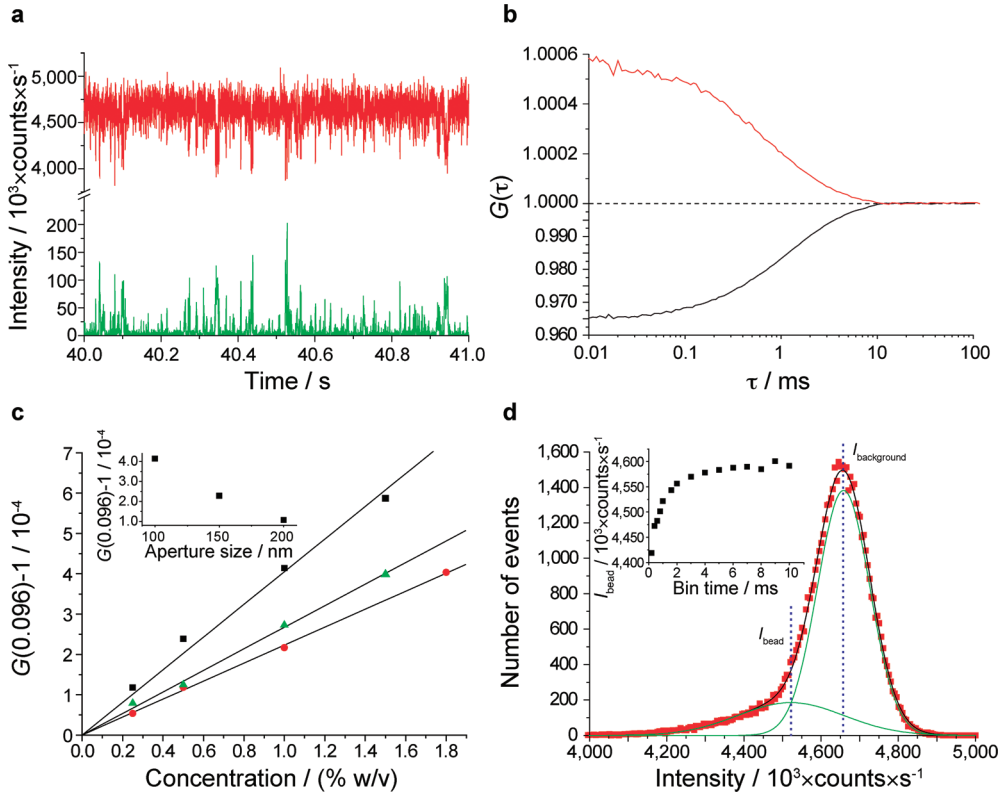

Figure 2. Proof-of-principle of single bead detection. (a) Time traces (100 μs bin-time, smoothed using seven-point second-order Savitzky–Golay algorithm) of a sample containing 1.5% (w/v) 24 nm diameter beads and 1 mM of Alexa Fluor 647 (background), recorded in a 100 nm aperture. Background and beads were excited at 633 and 488 nm, respectively. Red trace shows the background fluorescence and green trace the bead fluorescence. (b) Upper: temporal autocorrelation of the recorded background fluorescence in (a), subtracted with a corresponding measurement on a pure fluorophore solution. Lower: cross-correlation showing the anticorrelation between the two channels. (c) Amplitudes of the autocorrelation curves (value at τ = 96 μs) at different bead concentrations for 24 nm (■), 36 nm (●), and 110 nm (▲) diameter beads, in 100 , 150, and 200 nm apertures, respectively. Note that the molar concentrations are different for the different bead sizes. Black lines are linear regressions to the data. Inset: Autocorrelation amplitudes for 24 nm beads at 1% (w/v) in apertures of different sizes. (d) Intensity histogram of the background in (a) binned with 1 ms. Green lines show global fits of the histogram using two Gaussian functions. Vertical dashed blue lines indicate the intensities, I_{bead} and $I_{background}$, at the peak frequency for the two populations, with the intensity difference $\Delta I = I_{background} - I_{bead}$. Inset: influence of bin times (from 100 μs to 10 ms) on I_{bead}.

analysis can be combined with correlation analysis to provide robust multiparameter analysis.

Next, we performed measurements on solutions containing quantum dots (QDs) with a specified hydrodynamic diameter of 12 nm. Dual-color iFCCS experiments were used to distinctly prove QD detection and were compared with the corresponding autocorrelation curves (Figure 3a). The fact that QDs are smaller than fluorescent beads results in a smaller amplitude of the non-normalized (not shown) auto- and cross-correlation curves and a shorter diffusion time (Figures 2b and 3a). The ratio of the autocorrelation amplitudes of the corresponding background signals, $G(0)$-1, for the QD measurements and the 24 nm beads (eq S2, Supporting Information) yields V_{QD} = 1.0 ± 0.1 × 10^{-21} liters and an effective QD diameter of 12.6 ± 0.5 nm (assuming a spherical shape), i.e., in the range of the specified value of 12 nm. Based on the cross-correlation amplitude, assuming zero channel cross-talk, yields V_{QD} = 6.7 ± 0.8 × 10^{-22} liters and an effective QD diameter of 10.8 ± 0.5 nm.

The detection of individual protein molecules was demonstrated using allophycocyanin (APC), a ~104 kDa trimeric protein containing two phycocyanobilin chromophores per subunit rendering the protein strongly red fluorescent. This disk-like protein is approximately 11 nm in diameter and 3 nm thick.[34] Measurement on an APC solution shows an autocorrelation curve for the background signal and a distinct anticorrelation in the cross-correlation curve (Figure 3b). The anticorrelation amplitude provides a volume estimation of APC of V_{APC} = 2.5 × ± 0.6 × 10^{-22} liters, using the above approach, which is close to the V_{APC} = 2.8 × 10^{-22} liters calculated assuming the mentioned disk-like dimensions. Note that the non-normalized cross-correlation amplitudes for QDs and APC (Figure 3c) reveal the clear difference between their volumes, while a comparison of their diffusion coefficients, from the half amplitude of their standard FCS curves (Figure 3a,b, green dashed line), would suggest that QDs and APC have indistinguishable hydrodynamic radii.

Finally, we investigated ligand binding of a membrane protein, the pentameric $5HT_3$ receptor (M_w = 250 kDa), which was expressed heterologously in and extracted from mammalian cells.[35] Label-free detection of $5HT_3$ receptors ($5HT_3R$) dissolved in detergent micelles is demonstrated in Figure 4. The autocorrelation of the background fluorescence yields V_{5HT3R} = 4.9 ± 0.7 × 10^{-22} liters. This is in good agreement with the calculated volume of V_{5HT3R} = 4.9 × 10^{-22} liters for the receptor detergent complex, assuming a truncated conical shape of the receptor[36,37] surrounded by a 3 nm thick detergent torus[38] at the 5 nm diameter transmembrane region, yielding

dx.doi.org/10.1021/nl2036468 | Nano Lett. 2012, 12, 370–375

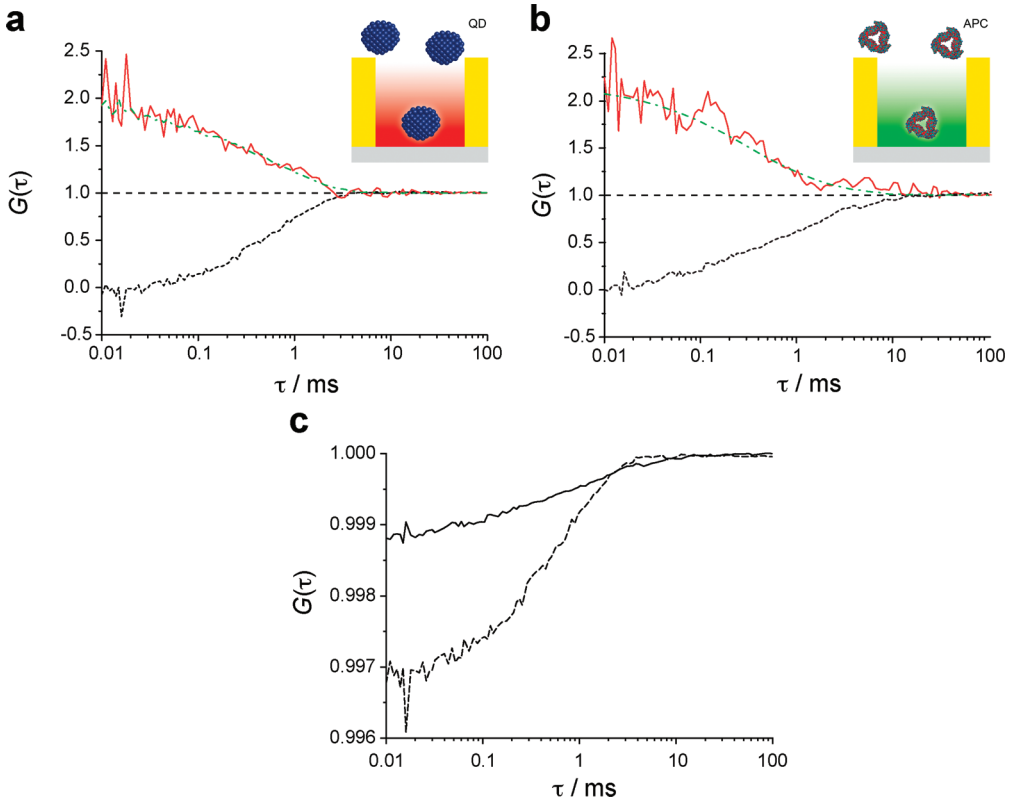

Figure 3. Analyzing quantum dots and proteins. (a) Normalized auto- (red line and green dashed line) and cross-correlation (black line) curves obtained from a dual-color measurement on a 6 μM of QDs (488 nm excitation) and 2 mM of Alexa Fluor 647 (background, 633 nm excitation) solution. The red solid line shows the autocorrelation of the background signal and the green dashed line the autocorrelation of the fluorescence signal from the QDs. Normalization factors for the background autocorrelation and the cross-correlation were 16 667 and 310, respectively. (b) Normalized autocorrelation curves for the background signal (red line) and fluorescence signal (green dashed line) and cross-correlation curve (black line) from a measurement on a 4 μM of allophycocyanin (APC, 633 nm excitation) and 2 mM of Alexa Fluor 488 (background, 488 nm excitation) solution. Normalization factors for the background autocorrelation and the cross-correlation were 12 500 and 833, respectively. (c) The non-normalized cross-correlation curves for the QD measurements in (a) (dashed line) and the APC measurements in (b) (solid), showing the amplitude ratio of ~2.7 which is the estimated volume difference between the QDs and APC. The background autocorrelation curves in (a) and (b) were subtracted with the corresponding normalized autocorrelation curve on a pure background solution. All measurements were performed in 100 nm apertures. In (a) and (b), the curves were normalized to facilitate the comparison of the correlation in the green and red channel.

3.1×10^{-22} and 1.8×10^{-22} liters for the volume of the protein and the detergent torus, respectively. The specific binding of the pharmaceutically active fluorescent ligand GR−Cy_3[35] to the $5HT_3R$ is also shown in Figure 4; the $5HT_3R$/GR−Cy_3 complex generates coinciding positive and negative fluorescence signals (compare with Figure 2a) and thus anticorrelated signals as a very clear proof of specific binding (Figure 4).[32] Note that the small GR−Cy_3 ligands do not modulate the background signal. For quantification of molecular interactions the concentrations of the interacting partners have to be adapted to the K_d values. In the case of the $5HT_3R$/GR−Cy_3, this value is in the nM range,[35] which allowed us to determine binding but not to quantify K_d. Attaching the smaller of the partners in the aperture will circumvent this limitation. Thereby the fluorescent background fluctuations and the corresponding iFCS curve would deliver binding kinetics, such as on- and off-time from which association/dissociation constants can be derived. The characterization of cell membrane proteins in the tiny volume of our nanostructured device opens new possibilities for analyzing components from individual cells, including markers facilitating detection of diseases,[39] determination of the amount of posttranslational labeled proteins,[37] or expression of recombinant proteins.[6]

In this work, we presented an approach for analyzing the volume, concentration, and motion of freely diffusing single protein molecules and nanoparticles in solution, with or without labeling. Our volume meter device was able to directly determine volumes of single proteins and nanoparticles smaller than 10^{-21} liters. To our knowledge this is the first direct determination of the volume of a protein molecule in solution, without any assumptions about molecular shape. The smallest protein we were able to detect was APC with a molecular mass of 100 kDa, which we consider as our current experimental detection limit. The theoretical detection limit for the method depends on several parameters, such as the size of the detection volume, the noise in the background fluorescence, and the concentration and the shape of the protein. Performing measurements in smaller apertures might allow detection of smaller proteins by increasing the V_{obj}/V_{dv}^{eff} ratio. Furthermore, using detectors that are able to measure higher photon fluxes would decrease the noise in the detected fluorescent background thereby improving the signal-to-noise ratio enabling smaller objects to be analyzed.

Here we used replacement of fluorescent background molecules as a contrast mechanism. However, the background signal can be any signal originating from the detection volume which is modified by objects diffusing through the detection

dx.doi.org/10.1021/nl2036468 | Nano Lett. 2012, 12, 370−375

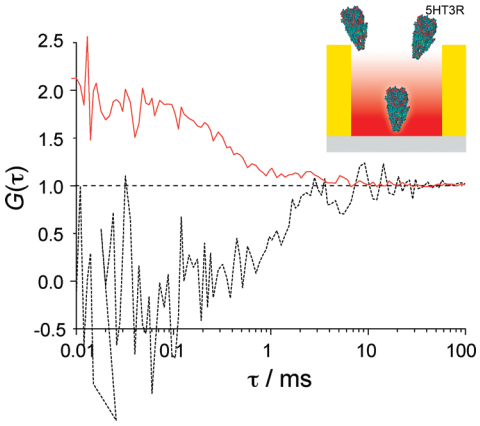

Figure 4. Ligand binding of the $5HT_3$ receptor. Normalized autocorrelation curve of the background signal (red line) and cross-correlation curve (black line) from a measurement on a solution containing 12 μM of $5HT_3$ receptor, 14 μM of the fluorescent ligand GR–Cy_3 (488 nm excitation), and 2 mM of Alexa Fluor 647 (background, 633 nm excitation) in a 100 nm aperture. The curves were normalized with normalization factors 10 000 and 4000 for the background autocorrelation and the cross-correlation, respectively, to facilitate the comparison of the correlation in the green and red channels.

volume, e.g., electrical, magnetic, or optical signals, which in the latter case might be a Raman signal from the replaced solvent molecules or simply light transmitted through the aperture. The small detection volume, here obtained by plasmonic nanostructures, enables the background signal to be sufficiently modulated by nanoscale objects. This principle has, e.g., been exploited in nanopore DNA sequencing, where an electrical current is characteristically modified by nucleotides passing the pore,[40] and for differentiation of protein analytes in hybrid biological solid-state nanopores.[41]

Our measurements were performed in one aperture at a time using a confocal microscope. However, parallel recordings are possible by, e.g., wide-field illumination of an array of apertures combined with CCD detection. Such a setup arrangement could simplify instrumentation, reduce cost, and enable miniaturization in form of a portable analysis device. Immobilization of molecules on the surface of the aperture would allow label-free study of transient binding/unbinding events of biomolecules or particles (viruses, phages, cell-derived organelles, and vesicles), such as ligand–receptor or antibody–antigen binding.

■ ASSOCIATED CONTENT

Supporting Information

Detailed description of experimental procedures, analysis procedures, and simulations of the electric field distribution inside subwavelength metal apertures. This material is available free of charge via the Internet at http://pubs.acs.org.

■ AUTHOR INFORMATION

Corresponding Author

*E-mail: horst.vogel@epfl.ch.

■ ACKNOWLEDGMENTS

Financial support was provided by the Swiss National Science Foundation to HV (SNF grant 31003A-118148) and the European Union for the Marie Curie Initial Training Network Experienced Researcher grant for T.S. We also thank Banafsheh Abasahl at the Nanophotonics and Metrology Laboratory, EPFL, for help with simulations, and Dr. Ruud Hovius, Laboratory of Physical Chemistry of Polymers and Membranes, EPFL, for providing the synthesized fluorescent ligand GR–Cy_3.

■ REFERENCES

(1) Majd, S.; Yusko, E. C.; Billeh, Y. N.; Macrae, M. X.; Yang, J.; Mayer, M. *Curr. Opin. Biotechnol.* **2010**, *21* (4), 439–476.
(2) Ahn, J.-H.; Kim, J.-H.; Reuel, N. F.; Barone, P. W.; Boghossian, A. A.; Zhang, J.; Yoon, H.; Chang, A. C.; Hilmer, A. J.; Strano, M. S. *Nano Lett.* **2011**, *11* (7), 2743–2752.
(3) Yanik, A. A.; Huang, M.; Kamohara, O.; Artar, A.; Geisbert, T. W.; Connor, J. H.; Altug, H. *Nano Lett.* **2010**, *10* (12), 4962–4969.
(4) Danelon, C.; Terrettaz, S.; Guenat, O.; Koudelka, M.; Vogel, H. *Methods* **2008**, *46* (2), 104–115.
(5) Kleefen, A.; Pedone, D.; Grunwald, C.; Wei, R.; Firnkes, M.; Abstreiter, G.; Rant, U.; Tampé, R. *Nano Lett.* **2010**, *10* (12), 5080–5087.
(6) Bill, R. M.; Henderson, P. J. F.; Iwata, S.; Kunji, E. R. S.; Michel, H.; Neutze, R.; Newstead, S.; Poolman, B.; Tate, C. G.; Vogel, H. *Nat. Biotechnol.* **2011**, *29* (4), 335–340.
(7) Liedberg, B.; Nylander, C.; Lundstrom, I. *Sens. Actuators* **1983**, *4* (2), 299–304.
(8) Bieri, C.; Ernst, O. P.; Heyse, S.; Hofmann, K. P.; Vogel, H. *Nat. Biotechnol.* **1999**, *17* (11), 1105–1108.
(9) Fan, X. D.; White, I. M.; Shopoua, S. I.; Zhu, H. Y.; Suter, J. D.; Sun, Y. Z. *Anal. Chim. Acta* **2008**, *620* (1–2), 8–26.
(10) Lomakin, A.; Benedek, G. B.; Teplow, D. B. Monitoring protein assembly using quasielastic light scattering spectroscopy. In *Amyloid, Prions, and Other Protein Aggregates*; Academic Press Inc: San Diego, CA, 1999; Vol. *309*, pp 429–459.
(11) Svergun, D. I.; Koch, M. H. J. *Rep. Prog. Phys.* **2003**, *66* (10), 1735–1782.
(12) Hahm, J.-i.; Lieber, C. M. *Nano Lett.* **2004**, *4* (1), 51–54.
(13) Garaj, S.; Hubbard, W.; Reina, A.; Kong, J.; Branton, D.; Golovchenko, J. A. *Nature* **2010**, *467* (7312), 190–193.
(14) Schneider, G. F.; Kowalczyk, S. W.; Calado, V. E.; Pandraud, G.; Zandbergen, H. W.; Vandersypen, L. M. K.; Dekker, C. *Nano Lett.* **2010**, *10* (8), 3163–3167.
(15) Merchant, C. A.; Healy, K.; Wanunu, M.; Ray, V.; Peterman, N.; Bartel, J.; Fischbein, M. D.; Venta, K.; Luo, Z.; Johnson, A. T. C.; Drndić, M. *Nano Lett.* **2010**, *10* (8), 2915–2921.
(16) Hall, A. R.; Scott, A.; Rotem, D.; Mehta, K. K.; Bayley, H.; Dekker, C. *Nat. Nano* **2010**, *5* (12), 874–877.
(17) Wennmalm, S.; Thyberg, P.; Xu, L.; Widengren, J. *Anal. Chem.* **2009**, *81* (22), 9209–9215.
(18) Hell, S. W. *Nat. Meth.* **2009**, *6* (1), 24–32.
(19) Laurence, T. A.; Weiss, S. *Science* **2003**, *299* (5607), 667–668.
(20) Genet, C.; Ebbesen, T. W. *Nature* **2007**, *445* (7123), 39–46.
(21) Levene, M. J.; Korlach, J.; Turner, S. W.; Foquet, M.; Craighead, H. G.; Webb, W. W. *Science* **2003**, *299* (5607), 682–686.
(22) Rigneault, H.; Capoulade, J.; Dintinger, J.; Wenger, J.; Bonod, N.; Popov, E.; Ebbesen, T. W.; Lenne, P. F. *Phys. Rev. Lett.* **2005**, *95*, (11), 117401.
(23) Liao, D.; Galajda, P.; Riehn, R.; Ilic, R.; Puchalla, J. L.; Yu, H. G.; Craighead, H. G.; Austin, R. H. *Opt. Express* **2008**, *16* (14), 10077–10090.
(24) Schwille, P.; Haupts, U.; Maiti, S.; Webb, W. W. *Biophys. J.* **1999**, *77* (4), 2251–2265.
(25) Sandén, T.; Salomonsson, L.; Brzezinski, P.; Widengren, J. *Proc. Natl. Acad. Sci. U.S.A.* **2010**, *107* (9), 4129–4134.
(26) Widengren, J.; Mets, U.; Rigler, R. *J. Phys. Chem.* **1995**, *99* (36), 13368–13379.
(27) Jankevics, H.; Prummer, M.; Izewska, P.; Pick, H.; Leufgen, K.; Vogel, H. *Biochemistry* **2005**, *44* (35), 11676–11683.

(28) Kask, P.; Palo, K.; Ullmann, D.; Gall, K. *Proc. Natl. Acad. Sci. U.S.A.* **1999**, *96* (24), 13756−13761.
(29) Chen, Y.; Muller, J. D.; So, P. T. C.; Gratton, E. *Biophys. J.* **1999**, *77* (1), 553−567.
(30) Schwille, P.; Meyer-Almes, F. J.; Rigler, R. *Biophys. J.* **1997**, *72* (4), 1878−1886.
(31) Persson, G.; Sandén, T.; Sandberg, A.; Widengren, J. *Phys. Chem. Chem. Phys.* **2009**, *11* (21), 4410−4418.
(32) Wennmalm, S.; Widengren, J. *Anal. Chem.* **2010**, *82* (13), 5646−5651.
(33) Palo, K.; Metz, U.; Jager, S.; Kask, P.; Gall, K. *Biophys. J.* **2000**, *79* (6), 2858−2866.
(34) Goldsmith, R. H.; Moerner, W. E. *Nat. Chem.* **2010**, *2* (3), 179−186.
(35) Wohland, T.; Friedrich, K.; Hovius, R.; Vogel, H. *Biochemistry* **1999**, *38* (27), 8671−8681.
(36) Unwin, N. *J. Mol. Biol.* **2005**, *346* (4), 967−989.
(37) Guignet, E. G.; Hovius, R.; Vogel, H. *Nat. Biotechnol.* **2004**, *22* (4), 440−444.
(38) Kunji, E. R. S.; Harding, M.; Butler, P. J. G.; Akamine, P. *Methods* **2008**, *46* (2), 62−72.
(39) Bernards, R. *Cell* **2010**, *141* (1), 13−17.
(40) Clarke, J.; Wu, H.-C.; Jayasinghe, L.; Patel, A.; Reid, S.; Bayley, H. *Nat. Nano* **2009**, *4* (4), 265−270.
(41) Yusko, E. C.; Johnson, J. M.; Majd, S.; Prangkio, P.; Rollings, R. C.; Li, J.; Yang, J.; Mayer, M. *Nat. Nano* **2011**, *6* (4), 253−260.

dx.doi.org/10.1021/nl2036468 | *Nano Lett.* 2012, 12, 370−375